IEEE Access
Multidisciplinary | Rapid Review | Open Access Journal

Received November 18, 2021, accepted January 16, 2022, date of publication January 18, 2022, date of current version January 27, 2022.

Digital Object Identifier 10.1109/ACCESS.2022.3144509

A High-Temperature and Frequency-Reconfigurable Multilayer Frequency Selective Surface Using Liquid Metal

PENG LI, (Member, IEEE), WEIGANG LIU, ZEMIN REN, WENJU MENG, AND LIWEI SONG

Key Laboratory of Electronic Equipment Structure Design, Ministry of Education, Xidian University, Xi'an 710071, China
Academy of Advanced Interdisciplinary Research, Xidian University, Xi'an 710126, China

Corresponding author: Peng Li (yinhong0523@163.com)

This work was supported by the National Natural Science Foundation of China (Grant No. 51875431, No. 61971334 and No.52035010), the Natural Science Basic Research Plan in Shaanxi Province (Grant No. 2021JZD-003 and No. 2021JM-121), the Fundamental Research Funds for the Central Universities, and the National 111 Project.

ABSTRACT A high-temperature and frequency-reconfigurable multilayer frequency selective surface (FSS) based on liquid metal is proposed in this work. After construction of a multilayer dielectric cavity with specific dielectric-shaped pillars and the injection of liquid metal (EGaIn) into each layer of the cavity, the liquid metal and dielectric pillars form a slot-type bandpass FSS, and frequency reconfiguration is realized by switching the injection layer. A prototype of the proposed FSS was designed, fabricated and measured. The measured results validated the design well. The good conductivity and fluidity of the liquid metal are utilized to realize the reconfigurable electromagnetic performance of the proposed FSS. This works in the C-band (5 GHz) and Ku band (13 GHz) and has a frequency switching time between 13.1 to 14.2 s. Moreover, due to the good thermal conductivity of liquid metal, the flowing liquid metal can take away heat, and the multilayer FSS can work as cooling plate. The heat transfer performance was investigated by numerical simulations. A 1000 ° plane heat source was set on the bottom surface of the double-layer FSS. The average temperature on the top surface was 62.2 °, when the liquid metal fluid in the FSS had a speed of 1 m/s. The proposed multilayer FSS has strong potential for applications in some special application fields involving stealth and hypersonic aircraft.

INDEX TERMS Multilayer FSS, frequency reconfiguration, liquid metal, heat transfer.

I. INTRODUCTION

A radome is an indispensable piece of equipment for airborne electronic systems, such as detection, navigation, communication and identification systems [1], [2]. With the rapid development of aerospace technology, aircraft radomes will soon face the large challenge of meeting the requirements for stealth and hypersonic capabilities. A frequency selective surface (FSS) is a kind of metasurface that can realize special electromagnetic performance, such as polarization manipulation [3], [4] and phase modulation [5]. FSS is a good technology for meeting the stealth requirement and has been used in the aircraft industry in recent years [6].

The associate editor coordinating the review of this manuscript and approving it for publication was Kuang Zhang.

The FSS is widely used in the fields of hybrid radomes [7], circuit analog absorbers [8], zigzag linear polarizers [9], etc., among which the most representative is the application to modern military technology such as stealth aircraft [10], [11]. Most typical FSSs are fabricated by laser etching, chemical etching or 3D printing FSS elements onto an existing single-sided copper clad laminate [12], [13]. Simultaneously, to adapt to complex and changeable service environments, a reconfigurable FSS has been proposed, the structure of which can be manually or automatically switched to match the current electromagnetic environment. Research on reconfigurable FSSs began in 1972 when Lee *et al.* designed a folded surface by loading lumped elements onto an FSS [14]. Azemi *et al.* used a metal resonant helix structure to control the stop band or pass band of an FSS by adjusting the height of the helix [15]. Ebrahimi *et al.* realized a second-order

bandpass FSS with an adjustable passband by using a varactor diode [16]. The former is a mechanically adjustable FSS, and the latter is an electronically controlled FSS. The devices used mainly include PIN diodes, varactor diodes and MEMS switches [17], [18]. Meanwhile, the hypersonic requirement results in high-temperature ablation (hundreds or even more than thousands of degrees). These current FSS technologies cannot meet the requirements of the high-temperature hypersonic working conditions.

Liquid metal has good fluidity and high thermal conductivity at room temperature. It has been used as the cooling medium for forced liquid cooling, which provides a solution to the ''thermal barrier'' problems caused by the high integration of electronic equipment and high-speed operation of packaging systems and hypersonic aircraft [19]. Moreover, liquid metal offers electrical conductivity. Therefore, it is not only applied in the fluid heat transfer field [20], [21] but also in the microwave electromagnetic field [22].

In 2009, scientists found that the liquid metal eutectic gallium-indium (EGaIn) is nontoxic and has all the electromagnetic characteristics needed by an antenna. Therefore, it is being researched as a promising new material for reconfigurable antennas [23]. Song *et al.* introduced liquid metal into a 3D printing microchannel to form an E-shaped patch antenna and realized multipolarization reconfiguration of the antenna by switching the continuous flow of liquid metal in the microchannels [24], [25]. Liu *et al.* injected liquid metal into a PDMS microchannel and placed it on a square substrate to form a slot antenna and achieved antenna frequency and polarization reconstruction by controlling the length and direction of liquid metal flow [26]. Chen *et al.* introduced liquid metal into a glass medium to form a dielectric resonant antenna and achieved $+45°$, $-45°$ and y-axis polarization reconstruction by controlling the channel and direction of flow of the liquid metal in the medium [27]. A pattern-reconfigurable Yagi-Uda antenna based on liquid metal was presented by Hao *et al.* [28]. The liquid metal alloy (LMA) was used to design a metasurface with switchable reflection phases, which serves as the superstrate of an antenna array to manipulate its scattering features [29]. Liquid metal can also be applied in FSS. Ghosh *et al.* described a miniaturized reconfigurable frequency selective surface, switching from allpass to bandpass/bandstop characteristic, depending on whether EGaIn is injected in the microchannels [30], [31]. Xu *et al.* presented a new implementation of liquid-metal-tuned higher-order bandpass frequency-selective surfaces capacitive-tuning slugs that are integrated into the resonant FSS layers [32], [33].

However, the above applications only use part of the properties of liquid metal; e.g., electrical conductivity and fluidity, or thermal conductivity and fluidity. There is no research on the application of all three properties to realize both electromagnetic and heat dissipation functions at the same time. This work proposes a reconfigurable bandpass slot-type multilayer liquid metal FSS that also has a high heat transfer capacity. Unlike the traditional FSS, this work uses all three properties of liquid metal: the electrical conductivity, fluidity and thermal conductivity. Therefore, the proposed multilayer FSS has good performance in both frequency selection and heat transfer and has strong potential for applications in specific scenarios; e.g., stealth and hypersonic aircraft.

II. MULTILAYER FSS ELEMENT DESIGN

The element structure diagram of the proposed frequency-reconfigurable multilayer liquid metal FSS is shown in Fig. 1. There are three substrates constituting a two-layer structure: the upper layer has four Y-shaped pillars, and the lower layer has one cross-shaped pillar. The center of each Y-shaped pillar is located at the center of the upper element of 1/4 size, and the center of the cross-shaped pillar is located at the center of the lower element. The cross-shaped pillar includes two branches, and the centers of the two branches overlap and are distributed in a connected structure at an angle of 90°. The Y-shaped pillar includes three branches, and the three branches are distributed in a connected structure of a circular array at an angle of 120°, with one of the branches parallel to the side boundary of the element. When the four side boundaries of each layer are sealed and the space between pillars and substrates is filled with liquid metal, the upper layer can work as a bandpass slot-type FSS at a specific frequency band, and the lower layer can function as an FSS at other frequency bands. Moreover, the liquid metal works as the electrical conductor, and the dielectric pillars work as slots. Other kinds of slot elements can also be adopted to replace the Y- or cross-shaped pillars.

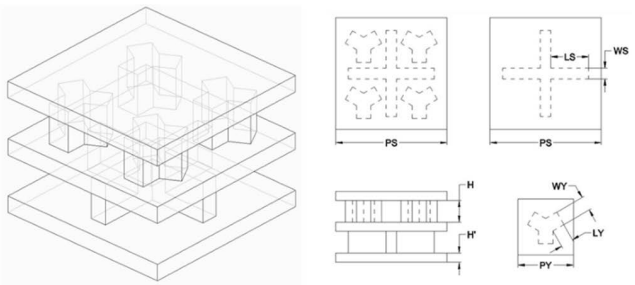

FIGURE 1. Frequency-reconfigurable double-layer FSS element structure diagram.

Each layer controls one specific frequency band. For example, in this work, if a C-band FSS is needed, the liquid metal is injected into the lower layer with the cross-shaped pillars and leaves the upper layer empty. If a Ku-band FSS is needed, the liquid metal is injected into the upper layer with the Y-shaped pillars and leaves the lower layer empty. When the liquid metal is switched among the different layers, the frequency reconfiguration of the FSS is realized. The switching time depends on the flow speed of the liquid metal and the total space volume between pillars.

The advantages of the proposed multilayer liquid metal FSS are significant: any classic slot FSS element can be employed, any range of the frequency band can be reconfigured, more layers (meaning more frequency bands) are easy

TABLE 1. Main dimensional parameters of the single- and double-layer FSSs (mm).

Parameter	Single layer	Double layer(Optimized)
PS	25.4	25.4
LS	8.4	8.6
WS	2.3	2.4
PY	12.7	12.7
LY	3.05	2.91
WY	2.6	3.26
H	5	5
H'	2	2

to realize, and reconfiguration of the other electromagnetic characteristics (such as the polarization) can be conveniently realized. Moreover, the liquid metal is a good heat conducting medium. If a fluid circuit is constructed and the dielectric material of the substrates and pillars is replaced with a high-temperature material (such as ceramics), the proposed liquid metal FSS can also be used as an efficient cooling plate and has strong potential applicability in high temperature environment, such as stealth and hypersonic aircraft.

III. DESIGN PARAMETER ANALYSIS

The basic design flow of the proposed multilayer liquid metal FSS is as follows: 1) define the specified frequency bands of the FSS; 2) select the number of layers and slot element type of each layer; 3) design the dimensional parameters of the pillar in each layer; and 4) optimize the parameters of all pillars in the multilayer FSS.

The specified frequency bands of this work are the C-band (5 GHz) and Ku-band (13 GHz). A double-layer FSS structure can meet the frequency requirements, and classic cross-shaped [34] and Y-shaped [35] slot elements (pillars) are adopted here for the C- and Ku-bands, respectively. There are four design parameters for the Y-shaped (WY and LY) and cross-shaped (LS and WS) pillars. There are two parameters for the distance between pillars (PS for cross-shaped and PY for Y-shaped), and two parameters for the heights of the substrate (H') and pillars (H). Considering cost and processing capability, polymethyl methacrylate (PMMA) is used as dielectric substrate and pillars instead of ceramics. Its permittivity is 2.57, and the loss tangent is 0.0078. The liquid metal is EGaIn (68.5% gallium, 21.5% indium, 10% tin), and the electrical conductivity is $6.8 \times 10\text{^}6$ Scotm^{-1}.

The design parameters of the pillar in single layer were simulated and designed by Ansys HFSS. S_{11} and S_{21} of every single layer are shown in Fig. 2 (solid lines), and the parameters are listed in Table 1 (single layer column). It is clear that the transmission performance of the two single-layer liquid metal FSSs is good.

The proposed two-layer frequency selective surface structure, when a single layer is filled with liquid metal, considers the vertical direction. The connected liquid metal increases

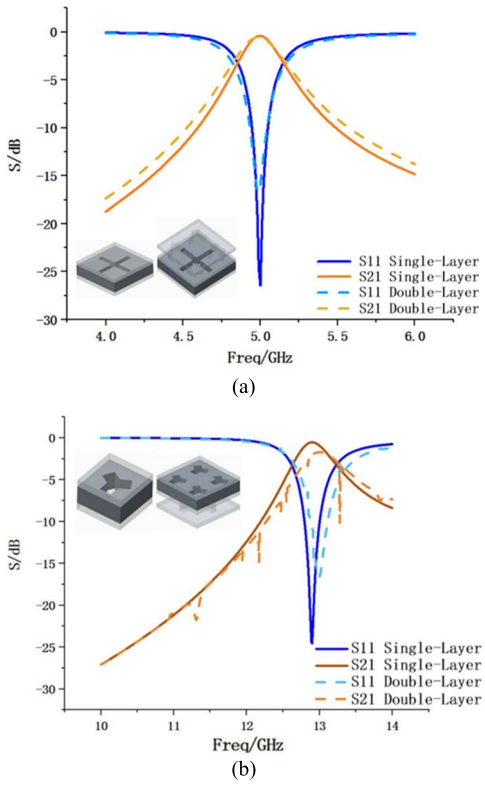

FIGURE 2. S_{11} and S_{21} of the single- and double-layer FSSs, (a) C-band, (b) Ku-band.

the effective inductance, while the consecutive Y- or cross-shaped pillars show large capacitance. To explain the resonance mechanism of the proposed FSS structure, simple circuit models are presented in Fig. 3. The design exhibits resonance in the form of a parallel combination (L_1- C_1) resulting in a bandpass response at 4.99 GHz when the frequency selective surface works in the C-band, and in the form of a parallel combination (L_2-C_2) resulting in a bandpass response at 12.98 GHz when the frequency selective surface works in the Ku-band. When the circuit models were implemented using Advanced Design System (ADS) software, the values of the lumped parameters were determined to be the followings: $L_1 = 76.75$ pH, $C_1 = 13.23$ pF, $L_2 = 24.36$ pH, and $C_2 = 6.17$ pF using the curve-fitting technique. The scattering parameters obtained from the circuit model were also compared with the simulated response as shown in Fig. 4, and they are in good agreement, thus validating the circuit model.

It is difficult to provide a set of equations relating the components of the electric circuit to the physical dimensions. But we can provide a set of qualitative relationships for changes in circuit element performance parameters as physical dimensions (LS, WS, LY, WY, H, and PS) change. When the proposed FSS works in C-band, C1 decreases and L1 increases when LS and WS increase. For Ku-band, when LY and WY increase, C2 decreases and L2 increases. As shown in Fig. 4 (c) and (d), the parameters L_1 and C_1 increase, the resonance frequency decreases. The same pattern is shown in Fig. 4 (e) and (f), when the parameters L_2 and C_2 are varied.

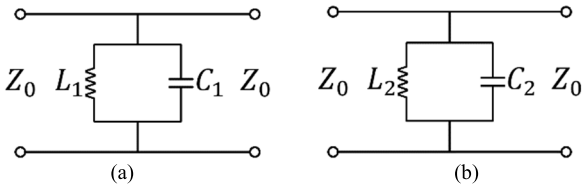

FIGURE 3. Equivalent circuit models of the proposed FSS, (a) C-band, (b) Ku-band.

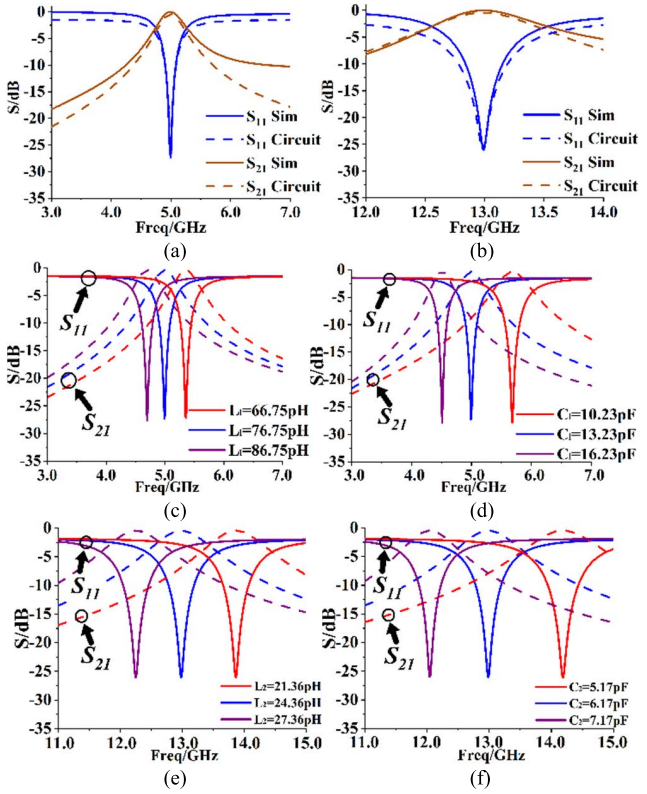

FIGURE 4. Comparison between simulation response and scattering parameters of circuit model, (a) C-band, (b) Ku-band; (c-f) S11 and S21 of the double-layer FSS when L_1, C_1, L_2, C_2 vary.

After the single cross-shaped layer (filled with liquid metal) is overlapped with the Y-shaped layer (no liquid metal filling) to form a double-layer FSS (working in the C-band), the transmission performance clearly degenerates, the resonance frequency shifts from 5.0 to 4.99 GHz, and the S_{11} value rises from −26.42 to −16.75 dB, as shown in Fig. 2 (a). When the single Y-shaped layer (filled with liquid metal) is overlapped with the cross-shaped layer (no liquid metal filling) to form the other double-layer FSS (working in the Ku-band), the transmission performance also degenerates, the resonance frequency shifts from 12.9 to 13.02 GHz, and the S_{11} value rises from −24.54 to −16.72 dB, as shown in Fig. 2 (b).

The reason for the above outcome is the interaction of different layers and asymmetric dielectrics on the two sides of the liquid metal. Therefore, based on the single FSS layers, the parameters of the entire multilayer FSS must be optimized. Before optimization, parameter analysis is necessary to define the key design parameters.

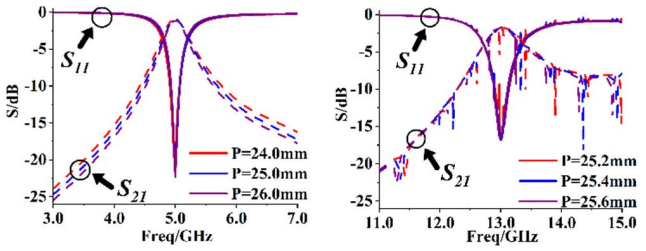

FIGURE 5. S_{11} and S_{21} of the double-layer FSS when PS/PY varies (C- and Ku-bands).

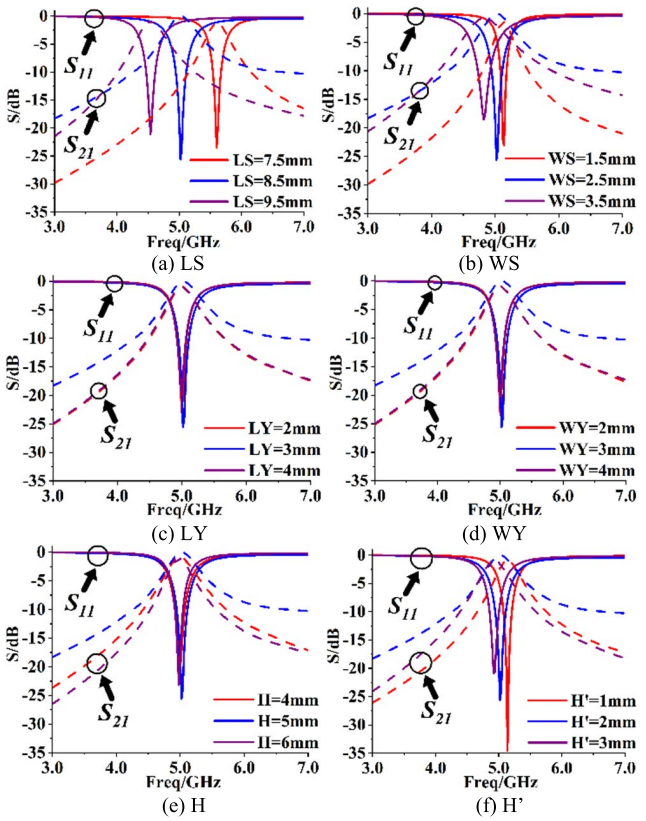

FIGURE 6. S_{11} and S_{21} of the double-layer FSS when LS, WS, LY, WY, H and H' vary (C-band).

The values in Table 1 (double layer column, optimized parameters) are the initial dimensions used in the parameter analysis at C-band, and the values in Table 1 (single layer column) are used at Ku-band. Figs. 3-5 plot the simulation results for the double-layer element when all parameters are altered. Fig. 5 shows S_{11} and S_{21} in both the C- and Ku-bands when the element space (PS/PY) varies. The element space has a negligible impact on the transmission performance. Fig. 6 shows the results when the other parameters (LS, WS, LY, WY, H and H') vary in the C-band, and Fig. 7 shows the results when the same parameters vary in the Ku-band. The conclusion is clear: the parameters LS and WS have major effects on S_{11} and S_{21} in the C-band (as shown in Fig. 6 (a) and (b)), and the parameters LY and WY have major effects on S_{11} and S_{21} in the Ku-band (as shown in Fig. 7 (c) and (d)). Parameter H has no effect on the results in

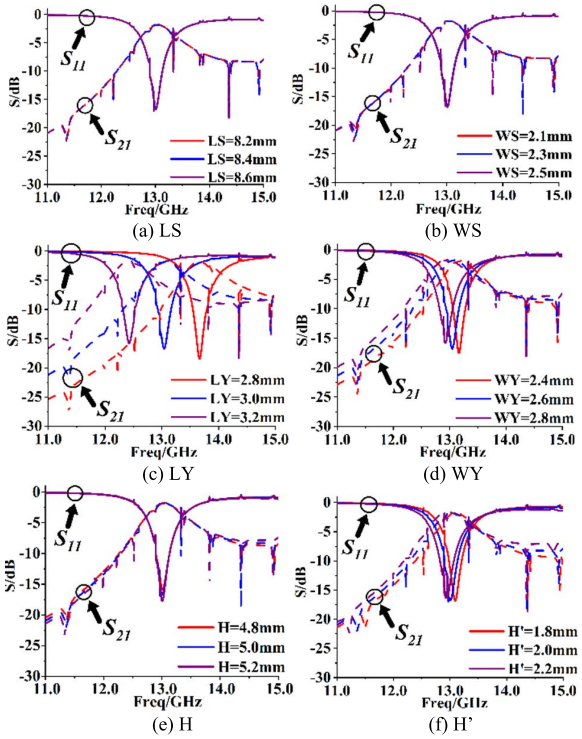

FIGURE 7. S_{11} and S_{21} of the double-layer FSS when LS, WS, LY, WY, H and H' vary (Ku-band).

either the C- or Ku-band (as shown in Fig. 6 (e) and Fig. 7 (e)), but H' has a minor impact on the results in both the C- and Ku-bands (as shown in Fig. 6 (f) and Fig. 7 (f)). Considering the fluidity of liquid metal, the height (H) of pillars cannot be too small; it is fixed to 5 mm, and H' is fixed to 2 mm. The element space parameters PS and PY are fixed to 25.4 mm and 12.7 mm for the cross-shaped and Y-shaped FSS layers, respectively. The sensitivity of these parameters is consistent before and after optimization. Thus, only four parameters (LS, WS, LY, and WY) need to be optimized.

Due to the considerable longitudinal dimension (H) of the proposed liquid metal double-layer FSS, the operation of the FSS for the case of large incident angles is investigated. To get the best transmission performance over a wide incident angle range, optimized parameters in Table 1 (double layer column) is used here. Three incident angles, 0°, 30° and 60° are considered for both the C- and Ku-bands. The S_{11} results are shown in Fig. 8. The frequency shift rate is only 1%, and the frequency shift value is 50 MHz (from 5.01 to 4.96 GHz) at C-band and 130 MHz (from 12.99 to 12.86 GHz) at Ku-band. Therefore, the considerable longitudinal dimension does not result in poor performance for oblique incidence at both C and Ku operation bands.

IV. PARAMETER OPTIMIZATION AND PROTOTYPE FABRICATION

To obtain the optimum parameters of the proposed liquid metal double-layer FSS, the particle swarm optimization (PSO) algorithm [36] is used here, which starts with a population randomly located in the search space.

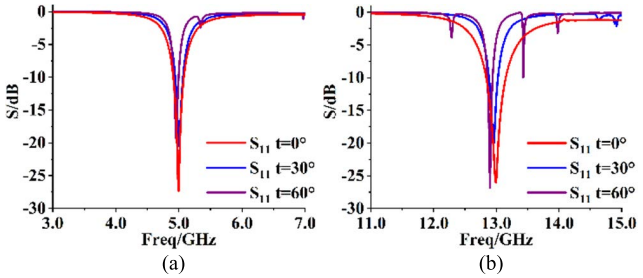

FIGURE 8. S_{11} of the double-layer FSS in different incident angles (a) C-band, (b) Ku-band.

The population of the potential solutions is called a swarm, and each individual solution within a swarm is called a particle. The optimization model can be described as follows:

$$\begin{aligned} &\text{Fine } (LS, WS, LY, WY) \\ &\text{Obj } \min \left(w_1 \left| f^C - f_0^C \right| + w_2 \left| f^{Ku} - f_0^{Ku} \right| \right) \\ &\quad \text{s.t. } S_{11} \le -20dB \\ &\qquad LS_{\min} \le LS \le LS_{\max} \\ &\qquad WS_{\min} \le WS \le WS_{\max} \\ &\qquad LY_{\min} \le LY \le LY_{\max} \\ &\qquad WY_{\min} \le WY \le WY_{\max} \end{aligned} \tag{1}$$

where LS, WS, LY, and WY are the design variables; the objective function is the minimum frequency shift between the request frequency (f_0) and simulated resonant frequency (f) at both the C- and Ku-bands; the superscripts C and Ku indicate the frequency band; w is the weight coefficient, and $w_1 = w_2 = 0.5$. The constraint conditions include S_{11} and the upper and lower bounds of the design variables. The swarm number is 40, and the iteration number is 30.

The resonant frequencies and S_{11} values of the three states (single layer, double layer before optimization and double layer after optimization) are listed in Table 2, and the optimized parameters are listed in Table 1 (double layer column). Clearly, the optimized liquid metal double-layer FSS has good performance in both the C- and Ku-bands. The S curves of the optimization results are plotted in Fig. 10 (dotted lines).

The best way to manufacture the prototype of the optimized liquid metal double-layer FSS is integrated forming, regarding which there is no need to worry about liquid metal leakage. However, due to the limitations of cost and fabrication, the prototype of the optimized liquid metal double-layer FSS was divided into three parts, as shown in Fig. 9 (a). The Y- and cross-shaped pillars were fabricated by a high-precision computerized numerical control (CNC) machine on PMMA substrates separately and finally assembled together. The liquid metal was injected into or extracted out of the PMMA layer by a peristaltic pump. The front and back sides of the prototype are illustrated in Fig. 9 (b), where the silver part is the liquid metal, and the transparent component is the PMMA. The cross-shaped and Y-shaped slots can be seen clearly. The size of the prototype is 300 mm × 300 mm. There are 20 × 20 Y-shaped pillars in

TABLE 2. Resonant frequencies and S11 values of the single- and double-layer FSSs before and after optimization.

Inject liquid metal into Y-shaped layer			
	single layer	double layer before optimization	double layer after optimization
resonant frequency/GHz	12.90	13.02	12.99
S_{11} value/dB	-24.54	-16.72	-26.05
Inject liquid metal in cross-shaped layer			
	single layer	double layer before optimization	double layer after optimization
resonant frequency/GHz	5.00	4.99	4.99
S_{11} value/dB	-26.42	-16.75	-27.36

the upper layer and 10 × 10 cross-shaped pillars in the lower layer. There are also inlet and outlet tubes for liquid metal to flow in and out in each layer. The dielectric substrates, seal washers and bolts are used to seal the cavity and prevent liquid leakage.

As a reconfigurable frequency selective surface, there is an inlet tube for liquid metal to flow in and an outlet tube for liquid metal to flow out in each layer; the diameter of both the inlet and outlet is 5 mm, and the fluid speed of liquid metal is 1 m/s. The time to fill or evacuate the upper FSS cavity is 13.1 s, and the time to fill or evacuate the lower FSS cavity is 14.2 s. Therefore, the switching time to reconfigure from C-band to Ku-band and from Ku-band to C-band is 14.2 s for FSS switch-overs.

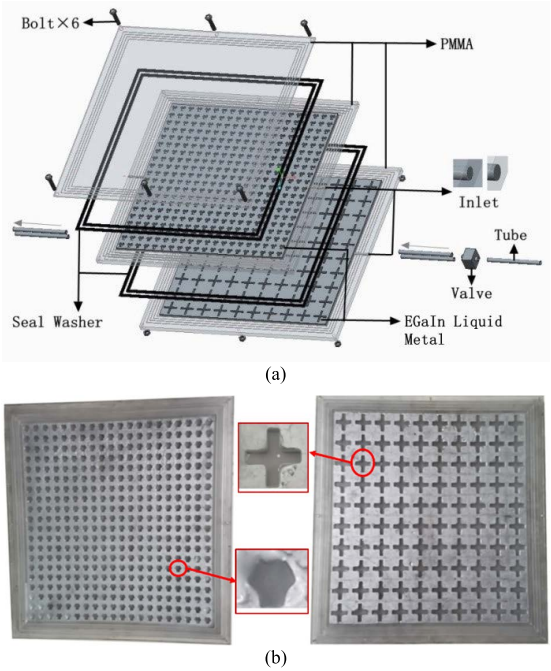

FIGURE 9. (a) Structure diagram and (b) photo of the liquid metal double-layer FSS prototype.

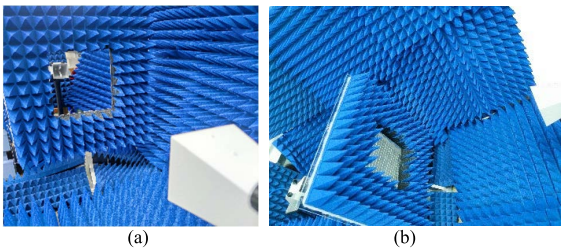

FIGURE 10. (a) Microwave measurement system and (b) the measured FSS.

V. MEASUREMENT AND DISCUSSION

The prototype was fabricated and the transmission performance (S11 and S21) was tested in an anechoic chamber. The measured two-frequency band working states are provided here for verification of the simulated results. The microwave measurement setups are shown in Fig 10. As shown in Fig. 10 (a), the standard-gain transmitting and receiving antennas (with operating frequency ranging from 2 to 18 GHz, double-ridged horn antenna) are fixed on the ground, and the fixture is fixed on the turntable to measure transmission coefficient at different angular incidences. The FSS is then embedded in the window of fixture (300 mm × 300 mm) to measure its transmission coefficient (see Fig. 10(b)). The center of antennas and FSS is located on the same horizontal line, and the distance between the fixture and each antenna is 800 mm. We measured the transmission between the transmitting antenna and the receiving antenna with/without the prototype, and the difference between the transmission results was regarded as the transmission performance.

Fig. 11 depicts a comparison between the measured (solid lines) and simulated (dotted line) S_{11} and S_{21} of the prototype. It shows that the measured resonant frequencies are 5.08 GHz in the C-band and 13.15 GHz in the Ku-band, and the corresponding S_{11} values are −35.86 and −30.45 dB, respectively. There is also some difference between the simulated and measured results. The frequency offset may be attributed to leakage from the gaps between the edges of the prototype, the finite size of the prototypes, and the fabricated tolerance of the prototypes. In particular, the contact surfaces between the liquid metal and PMMA pillars are rough due to the formation of some microbubbles or gaps, as shown in Fig. 9 (b). We can see that the edges of the metal slots are not smooth enough. In our opinion, this is the main reason for the frequency offset. In addition, some liquid metal drops remain in the upper layer when the liquid metal is pumped into the lower layer, which may also affect the measured results. Even so, the measured results still validate the design well.

The comparison with measured data varying the angle of incidence is shown in Fig. 12. The measured data deviates from the simulated data, and the angular stability is good for C-band and slightly worse for Ku-band. The frequency shift rate is 2.1% at C-band and 3% at Ku-band, the frequency shift value is 110 MHz (from 5.02 to 5.13 GHz) at C-band and 400 MHz (from 12.75 to 13.15 GHz) at Ku-band.

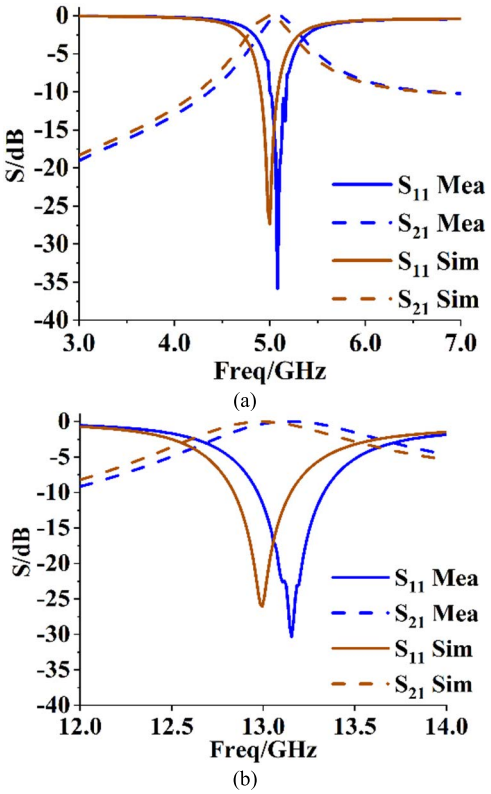

FIGURE 11. S_{11} and S_{21} of the measured and simulated results, (a) C-band, (b) Ku-band.

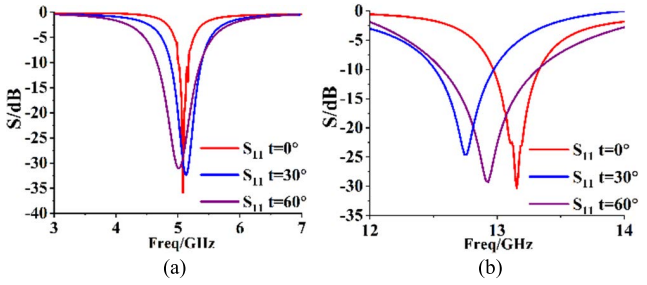

FIGURE 12. S_{11} of the measured results in different incident angles (a) C-band, (b) Ku-band.

VI. THERMAL ANALYSIS

As mentioned in the introduction, the proposed liquid metal double-layer FSS can meet the challenges of both stealth and hypersonic aircraft in the future. This section discusses verification of its heat transfer performance. The analysis was conducted via Ansys Icepak. The inlet of the liquid metal was in the left side and outlet in the right side. The material parameters used in the thermal analysis are listed in Table 3. A 1000 ° plane heat source, which corresponds to the aerodynamic heating temperature at a speed about 5 Ma, was set on the bottom surface of the double-layer FSS. Two fluids (liquid metal and air) were used for cooling the heat surface with an initial temperature 20 °. The fluid speed was fixed to 0.1 m/s. Four cases were studied here, 1) both Y- and cross-shaped layers are empty (air flows); 2) liquid metal flows in both Y- and cross-shaped layers; 3) liquid metal in the cross-shaped layer and air in Y-shaped layer; 4) liquid metal flows in the Y-shaped layer and air in cross-shaped layer. The average and maximum temperatures on the top surface of the 4 cases are listed in Table 4.

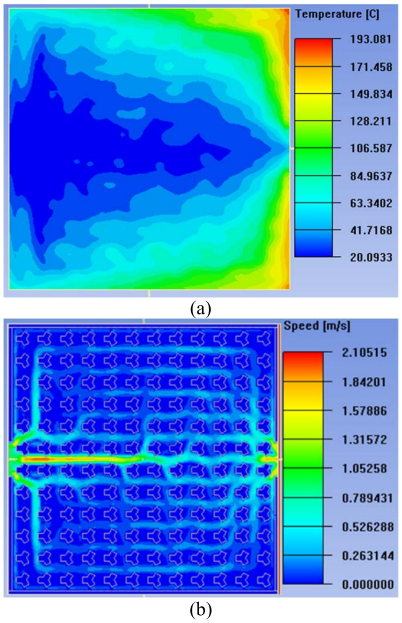

FIGURE 13. The temperature and fluid velocity nephograms of Case 4-HS, (a) temperature distribution on top surface, (b) speed distribution in Y-shaped layer.

TABLE 3. Material parameters of thermal analysis simulation.

Material	Density kg/m^3	heat capacity J/kg·K	Thermal conductivity W/m·K	Viscosity kg/m·s
EGaIn	6363	366	16.5	0.00222
Water	1000	4180	0.60	0.001
Ceramics (Al_2O_3)	3970	840	27.0	
Air	1.293	1005	0.0261	1.79e-5

TABLE 4. The average and maximum temperatures on the top surface (°).

Temperature	Case 1	Case 2	Case 3	Case 4	Case 4-HS
Average	998	550	862	338	62.2
Maximum	999.7	912.7	987.2	806.1	193.1

From Table 4, Case 4 has the best cooling results. The reasons for this are that the air (low thermal conductivity) flows in cross-shaped layer and insulates the heat source in the bottom of the same layer, and the liquid metal (high thermal conductivity and good fluidity) flows in the Y-shaped layer and cools the top surface.

It is well known that a higher fluid speed results in a higher cooling effect and lower temperature. The fluid speed of liquid metal rises to 1 m/s (marked as Case 4-HS in Table 4), and the average temperature is 62.2 °. This temperature is

TABLE 5. Comparison of the proposed liquid metal double-layer FSS with the literature.

Ref	Object of study	Reconfiguration category	Control method	Frequency/ GHz
[24]	Antennas	Polarization	EGaIn	2.4
[26]	Antennas	Frequency / polarization	EGaIn	LP: 2.03-2.28 CP: 2.3-3
[27]	Antennas	Polarization	EGaIn	2.4
[12]	FSS	NO		1.05
[13]	FSS	NO		9.18
[15]	FSS	Frequency	Spring	3-4
[16]	FSS	Frequency	VCD	5.2-3.7
[30]	FSS	Allpass to Bandpass/ Bandstop	EGaIn	Bandpass: 1.36 Bandstop: 2.63
[32]	FSS	Frequency	Galin-stan	8.6-9.2
[37]	FSS	Frequency	Water	5.2-7.0
This work	FSS	Frequency	EGaIn	5/13

less than 80 °, which is the maximum working temperature for most electronic device. Hence, the proposed liquid metal double-layer FSS has a good cooling effect and application potential in hypersonic aircraft. The temperature and fluid speed nephograms of Case 4-HS are shown in Fig. 13 for reference.

VII. CONCLUSION

A frequency-reconfigurable liquid metal multilayer FSS was proposed, designed, fabricated, and measured in this work. Table 5 compares the proposed liquid metal FSS with other reconfigurable FSSs or antennas from prior works. It is clear from the table that none of the prior works utilized good electrical conductivity, fluidity and thermal conductivity of liquid metal to realize both the reconfigurable electromagnetic performance and heat transfer capability achieved in this work. Therefore, it can be used in certain special application fields. Its advantages are summarized as follows:

1) It has both good frequency selective performance and good capability for achieving satisfactory heat transfer performance. Therefore, it can meet the challenges of stealth and hypersonic aircraft in the future.

2) It easily switches from C-band to Ku-band or from Ku-band to C-band. It also has potential to realize the reconfiguration of additional EM performance factors; e.g., polarization.

3) Any type of classic and advanced slot FSS elements can be used in the proposed liquid metal FSS and achieve different EM performance or functional combinations.

4) To achieve a better cooling effect, two fluids (air and liquid metal) can be used together where air flows in the layer which is close to the heat source, and liquid metal flows in the other layer.

REFERENCES

[1] W. Xu, Y. Zong, P. Li, and Y. Qiu, "Variable thickness airborne radome design considering thickness profile control and additional electromagnetic performance," *IEEE Trans. Antennas Propag.*, vol. 69, no. 4, pp. 2443–2448, Apr. 2021.

[2] W. Xu, B. Y. Duan, P. Li, and Y. Qiu, "Study on the electromagnetic performance of inhomogeneous radomes for airborne applications—Part II: The overall comparison with variable thickness radomes," *IEEE Trans. Antennas Propag.*, vol. 65, no. 6, pp. 3175–3183, Jun. 2017.

[3] Y. Yuan, K. Zhang, X. Ding, B. Ratni, S. N. Burokur, and Q. Wu, "Complementary transmissive ultra-thin meta-deflectors for broadband polarization-independent refractions in the microwave region," *Photon. Res.*, vol. 7, no. 1, pp. 80–88, 2019.

[4] K. Zhang, Y. Yuan, X. Ding, H. Li, B. Ratni, Q. Wu, J. Liu, S. N. Burokur, and J. Tan, "Polarization-engineered noninterleaved metasurface for integer and fractional orbital angular momentum multiplexing," *Laser Photon. Rev.*, vol. 15, no. 1, pp. 1–10, Jan. 2021.

[5] Y. Yuan, K. Zhang, B. Ratni, Q. Song, X. Ding, Q. Wu, S. N. Burokur, and P. Genevet, "Independent phase modulation for quadruplex polarization channels enabled by chirality-assisted geometric-phase metasurfaces," *Nature Commun.*, vol. 11, no. 1, pp. 1–9, 2020.

[6] P. C. Kim, D. G. Lee, I. S. Seo, and G. H. Kim, "Low-observable radomes composed of composite sandwich constructions and frequency selective surfaces," *Compos. Sci. Technol.*, vol. 68, no. 9, pp. 2163–2170, 2008.

[7] M.-S. Kim and S.-S. Kim, "Design and fabrication of 77-GHz radar absorbing materials using frequency-selective surfaces for autonomous vehicles application," *IEEE Microw. Wireless Compon. Lett.*, vol. 29, no. 12, pp. 779–782, Dec. 2019.

[8] Y. Zhao, Y. Li, and G. Yang, "A novel wideband absorptive frequency selective surface based on circuit analog absorber," *Acta Phys. Sinica*, vol. 69, no. 19, 2020, Art. no. 198101.

[9] E. Arnieri, F. Greco, L. Boccia, and G. Amendola, "A SIW-based polarization rotator with an application to linear-to-circular dual-band polarizers at $K - /Ka$-band," *IEEE Trans. Antennas Propag.*, vol. 68, no. 5, pp. 3730–3738, May 2020.

[10] P. C. Kim, D. G. Lee, I. S. Seo, and G. H. Kim, "Nanocomposite stealth radomes with frequency selective surfaces," *Composite Struct.*, vol. 86, nos. 1–3, pp. 299–305, Nov. 2008.

[11] P. C. Kim, D. G. Lee, W.-G. Lim, and I. S. Seo, "Polarization characteristics of a composite stealth radome with a frequency selective surface composed of dipole elements," *Compos. Struct.*, vol. 90, no. 2, pp. 242–246, Sep. 2009.

[12] S. Ghosh and S. Lim, "A miniaturized bandpass frequency selective surface exploiting three-dimensional printing technique," *IEEE Antennas Wireless Propag. Lett.*, vol. 18, no. 7, pp. 1322–1326, Jul. 2019.

[13] S. Chen, T. Pan, Z. Yan, L. Dai, Y. Peng, M. Gao, and Y. Lin, "Flexible serpentinelike frequency selective surface for conformal applications with stable frequency response," *IEEE Antennas Wireless Propag. Lett.*, vol. 18, no. 7, pp. 1477–1481, Jul. 2019.

[14] S. W. Lee and T. T. Fong, "Electromagnetic wave scattering from an active corrugated structure," *J. Appl. Phys.*, vol. 43, no. 2, pp. 388–396, Feb. 1972.

[15] S. N. Azemi, K. Ghorbani, and W. S. T. Rowe, "A reconfigurable FSS using a spring resonator element," *IEEE Antennas Wireless Propag. Lett.*, vol. 12, pp. 781–784, 2013.

[16] A. Ebrahimi, Z. Shen, W. Withayachumnankul, S. F. Al-Sarawi, and D. Abbott, "Varactor-tunable second-order bandpass frequency-selective surface with embedded bias network," *IEEE Trans. Antennas Propag.*, vol. 64, no. 5, pp. 1672–1680, May 2016.

[17] B. Philips, E. A. Parker, and R. J. Langley, "Active FSS in an experimental horn antenna switchable between two beamwidths," *Electron. Lett.*, vol. 31, no. 1, pp. 1–2, Jan. 1995.

[18] M. Safari, C. Shafai, and L. Shafai, "X-band tunable frequency selective surface using MEMS capacitive loads," *IEEE Trans. Antennas Propag.*, vol. 63, no. 3, pp. 1014–1021, Mar. 2015.

[19] A. Sakanova, C. F. Tong, K. J. Tseng, R. Simanjorang, and A. K. Gupta, "Weight consideration of liquid metal cooling technology for power electronics converter in future aircraft," in *Proc. IEEE 2nd Annu. Southern Power Electron. Conf. (SPEC)*, Dec. 2016, pp. 1–5.

[20] Y. Yerasimou, V. Pickert, S. Dai, and Z. Wang, "Thermal management system for press-pack IGBT based on liquid metal coolant," *IEEE Trans. Compon., Packag., Manuf. Technol.*, vol. 10, no. 11, pp. 1849–1860, Nov. 2020.

[21] R. Zhang, M. Hodes, N. Lower, and R. Wilcoxon, "Thermo-fluid characteristics of a minichannel heat sink cooled with liquid metal," in *Proc. 29th IEEE Semiconductor Thermal Meas. Manage. Symp.*, Mar. 2013, pp. 159–165.

[22] B. L. Cumby, D. B. Mast, C. E. Tabor, M. D. Dickey, and J. Heikenfeld, "Robust pressure-actuated liquid metal devices showing reconfigurable electromagnetic effects at GHz frequencies," *IEEE Trans. Microw. Theory Techn.*, vol. 63, no. 10, pp. 3122–3130, Oct. 2015.
[23] J.-H. So, J. Thelen, A. Qusba, G. J. Hayes, G. Lazzi, and M. D. Dickey, "Reversibly deformable and mechanically tunable fluidic antennas," *Adv. Funct. Mater.*, vol. 19, no. 22, pp. 3632–3637, 2009.
[24] L. Song, W. Gao, and Y. Rahmat-Samii, "3-D printed microfluidics channelizing liquid metal for multipolarization reconfigurable extended E-shaped patch antenna," *IEEE Trans. Antennas Propag.*, vol. 68, no. 10, pp. 6867–6878, Oct. 2020.
[25] L. Song, W. Gao, C. O. Chui, and Y. Rahmat-Samii, "Wideband frequency reconfigurable patch antenna with switchable slots based on liquid metal and 3-D printed microfluidics," *IEEE Trans. Antennas Propag.*, vol. 67, no. 5, pp. 2886–2895, May 2019.
[26] Y. Liu, Q. Wang, Y. Jia, and P. Zhu, "A frequency- and polarization-reconfigurable slot antenna using liquid metal," *IEEE Trans. Antennas Propag.*, vol. 68, no. 11, pp. 7630–7635, Nov. 2020.
[27] Z. Chen, H. Wong, and J. Kelly, "A polarization-reconfigurable glass dielectric resonator antenna using liquid metal," *IEEE Trans. Antennas Propag.*, vol. 67, no. 5, pp. 3427–3432, May 2019.
[28] J. Hao, J. Ren, X. Du, J. H. Mikkelsen, M. Shen, and Y. Zeng Yin, "Pattern-reconfigurable Yagi–Uda antenna based on liquid metal," *IEEE Antennas Wireless Propag. Lett.*, vol. 20, no. 4, pp. 587–591, Apr. 2021.
[29] Y. Liu, Z. Liu, Q. Wang, and Y. Jia, "Low-RCS antenna array with switchable scattering patterns employing microfluidic liquid metal alloy-based metasurface," *IEEE Trans. Antennas Propag.*, vol. 69, no. 12, pp. 8955–8960, Dec. 2021.
[30] S. Ghosh and S. Lim, "A multifunctional reconfigurable frequency-selective surface using liquid-metal alloy," *IEEE Trans. Antennas Propag.*, vol. 66, no. 9, pp. 4953–4957, Sep. 2018.
[31] S. Ghosh, S. I. H. Shah, and S. Lim, "Bistate frequency selective surface based on microfluidic technology," in *Proc. IEEE Int. Symp. Antennas Propag. USNC/URSI Nat. Radio Sci. Meeting*, Jul. 2018, pp. 2045–2046.
[32] K. Xu, J. H. Choi, K. Payne, J. K. Lee, and J.-B. Lee, "Flexible liquid metal frequency selective surface with tunable second-order bandpass response," in *Proc. IEEE Int. Symp. Antennas Propag. North Amer. Radio Sci. Meeting*, Jul. 2020, pp. 725–726.
[33] K. Xu and J. H. Choi, "Flexible liquid-metal-tuned higher-order bandpass frequency selective surfaces," in *Proc. IEEE Asia–Pacific Microw. Conf. (APMC)*, Dec. 2020, pp. 296–298.
[34] R. Shavit, *Radome Electromagnetic Theory and Design*. Hoboken, NJ, USA: Wiley, 2018, pp. 39–88.
[35] B. Gao, S. Huang, Z. Ren, Y. Chen, and X. Wang, "Design and verification of an integrated free-standing thick-screen FSS radome," *IEEE Antennas Wireless Propag. Lett.*, vol. 17, no. 9, pp. 1630–1634, Sep. 2018.
[36] W. Xu, B. Y. Duan, P. Li, N. Hu, and Y. Qiu, "Multiobjective particle swarm optimization of boresight error and transmission loss for airborne radomes," *IEEE Trans. Antennas Propag.*, vol. 62, no. 11, pp. 5880–5885, Nov. 2014.
[37] X. Yan, X. Kong, Q. Wang, L. Xing, F. Xue, Y. Xu, S. Jiang, and X. Liu, "Water-based reconfigurable frequency selective rasorber with thermally tunable absorption band," *IEEE Trans. Antennas Propag.*, vol. 68, no. 8, pp. 6162–6171, Aug. 2020.

PENG LI (Member, IEEE) was born in 1981. He received the B.S. and Ph.D. degrees in mechanical engineering from Xidian University, Xi'an, China, in 2003 and 2011, respectively.

From 2015 to 2016, he was a Visiting Scholar with the Department of Electrical and Computer Engineering, University of Alberta, Edmonton, AB, Canada. He is currently a Professor with the School of Electromechanical Engineering, Xidian University. His current research interests include numerical computation and optimization design of mechanical-electromagnetic-thermal problems of electronic equipments.

WEIGANG LIU was born in 1997. He received the bachelor's degree from the Hefei University of Technology, China, in 2019. He is currently pursuing the master's degree with the Key Laboratory of Electronic Equipment Structure Design, Ministry of Education, Xidian University, China.

His research interests include electromechanical coupling and design of reconfigurable frequency selection selective.

ZEMIN REN was born in 1996. He is currently pursuing the master's degree with the Key Laboratory of Electronic Equipment Structure Design, Ministry of Education, Xidian University, China.

His research interests include conformal load-bearing antenna array and 3-D printing.

WENJU MENG was born in 1995. He received the bachelor's degree from the Anyang Institute of Technology, China, in 2019. He is currently pursuing the master's degree with the Key Laboratory of Electronic Equipment Structure Design, Ministry of Education, Xidian University, China.

His research interest includes the optimization design of the channel topology for frequency selection surface.

LIWEI SONG was born in Inner Mongolia, China, in 1981. He received the B.S. degree in applied physics and the Ph.D. degree in mechanical engineering from Xidian University, Xi'an, China, in 2004 and 2011, respectively.

Since 2011, he has been with the Key Laboratory of Electronic Equipment Structure Design, Ministry of Education, Xidian University, where he is currently an Associate Professor with the School of Electromechanical Engineering. From August 2014 to August 2015, he was a Visiting Scholar with the School of Electrical and Computer Engineering, RMIT University, Australia. His major research interests include coupled mechanical-electromagnetic-thermal problems in the radar antenna, integrated design of coupled mechanical-electromagnetic-thermal problems, and the compensation methods of the distorted radar antenna.